ORIGINAL ARTICLE

Multiparametric Analysis Combining DSC-MR Perfusion and [18F]FET-PET is Superior to a Single Parameter Approach for Differentiation of Progressive Glioma from Radiation Necrosis

Jürgen Panholzer[1,2] · Gertraud Malsiner-Walli[3] · Bettina Grün[3] · Ognian Kalev[4] · Michael Sonnberger[5] · Robert Pichler[6,7,8]

Abstract

Purpose Perfusion-weighted (PWI) magnetic resonance imaging (MRI) and O-(2-[18F]fluoroethyl-)-l-tyrosine ([18F]FET) positron emission tomography (PET) are both useful for discrimination of progressive disease (PD) from radiation necrosis (RN) in patients with gliomas. Previous literature showed that the combined use of FET-PET and MRI-PWI is advantageous; hhowever the increased diagnostic performances were only modest compared to the use of a single modality. Hence, the goal of this study was to further explore the benefit of combining MRI-PWI and [18F]FET-PET for differentiation of PD from RN. Secondarily, we evaluated the usefulness of cerebral blood flow (CBF), mean transit time (MTT) and time to peak (TTP) as previous studies mainly examined cerebral blood volume (CBV).

Methods In this single center study, we retrospectively identified patients with WHO grades II–IV gliomas with suspected tumor recurrence, presenting with ambiguous findings on structural MRI. For differentiation of PD from RN we used both MRI-PWI and [18F]FET-PET. Dynamic susceptibility contrast MRI-PWI provided normalized parameters derived from perfusion maps (r(relative)CBV, rCBF, rMTT, rTTP). Static [18F]FET-PET parameters including mean and maximum tumor to brain ratios (TBR_{mean}, TBR_{max}) were calculated. Based on histopathology and radioclinical follow-up we diagnosed PD in 27 and RN in 10 cases. Using the receiver operating characteristic (ROC) analysis, area under the curve (AUC) values were calculated for single and multiparametric models. The performances of single and multiparametric approaches were assessed with analysis of variance and cross-validation.

Results After application of inclusion and exclusion criteria, we included 37 patients in this study. Regarding the in-sample based approach, in single parameter analysis $rTBR_{mean}$ (AUC $= 0.91$, $p < 0.001$), $rTBR_{max}$ (AUC $= 0.89$, $p < 0.001$), rTTP (AUC $= 0.87$, $p < 0.001$) and $rCBV_{mean}$ (AUC $= 0.84$, $p < 0.001$) were efficacious for discrimination of PD from RN. The $rCBF_{mean}$ and rMTT did not reach statistical significance. A classification model consisting of TBR_{mean}, $rCBV_{mean}$ and rTTP achieved an AUC of 0.98 ($p < 0.001$), outperforming the use of $rTBR_{mean}$ alone, which was the single parametric approach with the highest AUC. Analysis of variance confirmed the superiority of the multiparametric approach over the single parameter one ($p = 0.002$). While cross-validation attributed the highest AUC value to the model consisting of TBR_{mean} and $rCBV_{mean}$, it also suggested that the addition of rTTP resulted in the highest accuracy. Overall, multiparametric models performed better than single parameter ones.

✉ Jürgen Panholzer
juergen.panholzer@kepleruniklinikum.at

1 Department of Neurology, Kepler University Hospital, Linz, Austria

2 Faculty of Medicine, Johannes Kepler University, Linz, Austria

3 Institute for Statistics and Mathematics, WU University of Economics and Business, Vienna, Austria

4 Department for Pathology and Molecular Pathology, Neuromed Campus, Kepler University Hospital, Linz, Austria

5 Department for Neuroradiology, Neuromed Campus, Kepler University Hospital, Linz, Austria

6 Department for Nuclear Medicine, Neuromed Campus, Kepler University Hospital, Linz, Austria

7 Institute of Nuclear Medicine, Steyr Hospital, Steyr, Austria

8 Department of Radiology, Clinic of Nuclear Medicine, Medical University Graz, Graz, Austria

Conclusion   A multiparametric MRI-PWI and [18F]FET-PET model consisting of TBR$_{mean}$, rCBV$_{mean}$ and PWI rTTP significantly outperformed the use of rTBR$_{mean}$ alone, which was the best single parameter approach. Secondarily, we firstly report the potential usefulness of PWI rTTP for discrimination of PD from RN in patients with glioma; however, for validation of our findings the prospective studies with larger patient samples are necessary.

Keywords   Astrocytoma · Pseudoprogression · Amino acid PET · Perfusion maps · Radiation therapy

Introduction

Next to surgery and chemotherapy, radiation is part of standard treatment in patients with glioma [1]. Postradiation effects include radiation necrosis (RN) and pseudoprogression, manifesting as magnetic resonance imaging (MRI) T1-postgadolinium contrast enhancement [2]. While RN represents a necrotic local tissue reaction to radiation, pseudoprogression may constitute an overresponse to therapy [3]. The Response Assessment in Neuro-Oncology (RANO) group proposed structural MRI including diffusion-weighted imaging (DWI) as standard protocol for glioma assessment [4]; however, postradiation features seen in structural MRI often overlap with those of progressive disease (PD), limiting the accuracy [5].

As, opposed to necrotic tissue, PD is characterized by hypervascularization and hypercellularity, MRI perfusion-weighted imaging (PWI) and DWI provide additional information for differentiation. Prior studies confirmed the usefulness of dynamic susceptibility contrast-enhanced (DSC) MRI perfusion-derived CBV and ADC increasing the specificity for differentiation of RN from PD [6]. While the efficacy of MRI-PWI is generally accepted, some results are conflicting as for instance Boxerman et al. could not differentiate treatment-related changes from PD on the basis of initial CBV measurement alone [7]. While some authors reported the usefulness of specific thresholds for CBV for differentiation of treatment-related changes from PD [8], others claimed the opposite [9] and stated a dependence of CBV on MGMT promotor methylation [10]. The CBV measurements may be heterogeneously distributed in recurrent lesions [9, 11] and overlap between PD and treatment-related changes [12, 13]. The nonquantitative nature and lack of complete lesion coverage in the presence of susceptibility artefacts limit the DSC MRI perfusion method [14–16].

Another modality to distinguish RN from PD is using radiolabeled amino acids like O-(2-[18F]fluoroethyl-)-L-tyrosine ([18F]FET) [17]. After passing through the blood-brain barrier, [18F]FET is transferred into cells by amino acid transporters. This transfer is measured by positron emission tomography (PET) [18]. Overall, previous studies accredited [18F]FET-PET (using TBR = tumor to brain ratio) superior accuracy for differentiation of RN from PD compared to MRI-PWI (CBV) [17, 19, 20]. A few studies showed increased diagnostic performance when combining MRI-PWI with [18F]FET-PET for differentiation of RN from PD, and only under specific circumstances or with at best modest benefit [17, 19].

In summary, previous literature suggests that both MRI-PWI and [18F]FET-PET are potentially useful for differentiation of RN from PD in glioma patients. While, overall, current literature indicates [18F]FET-PET to be superior and combination with MRI-PWI may slightly increase diagnostic performance as discussed above. Ultimately, the overall benefit of combining MRI-PWI with [18F]FET-PET for differentiation of RN from PD compared to using a single modality is not clear to this day. Therefore, in this single center study, we evaluated the potential of multiparametric analysis combining MRI-PWI with [18F]FET-PET. Secondarily, we assessed the usefulness of cerebral blood flow (CBF), mean transit time (MTT) and time to peak (TTP) as previous studies mainly examined cerebral blood volume (CBV).

Methods

Patient Population

From our database, we retrospectively identified all [18F]FET-PET brain scans ($n = 411$) performed between January 2016 and July 2021 at Neuromed Campus, Kepler University Hospital Linz, Austria. Further selection was based on the criteria and patients' digital records stated below. We conducted this study according to ethical principles of the Declaration of Helsinki.

Inclusion Criteria

1. Adult patients (>18 years) with histopathological verified glioma (WHO grades II, III or IV) according to the WHO 2016 classification.
2. Referral for [18F]FET-PET for differentiation between PD and RN due to previous MRI findings suspicious for PD according to RANO [21].
3. Previous radiotherapy as part of the standard therapy of patients with glioma.

Exclusion Criteria

1. > 2 months between initial PET and previous MRI scan.
2. Change in therapy or surgery of the target lesion after initial scans in the examined period.
3. Lack of histopathological, radiological, and clinical follow-up and therefore compromised outcome evaluation.

MRI Protocol

Except for one patient, all scans were obtained from a single MRI scanner (3 Tesla Skyra®, Siemens, Munich, Germany). For the remaining patient, scans were obtained from another device (3 Tesla Verio®, Siemens). Scanning parameters for all sequences are available in the supplement (file name = cross-validation). A prebolus was applied before administration of the main bolus via intravenous route (gadolinium-based agent, 0.1 ml/kg body weight; infusion rate, 5 ml/s followed by 25 ml of NaCl). Structural MRI scans based on T2 and contrast-enhanced T1 sequences were obtained. Perfusion maps were generated by Syngo MR Neuro Perfusion Engine® (Siemens, Munich, Germany). We performed postprocessing leakage correction based on the Boxerman-Weisskoff method [22].

[18F]FET PET Protocol

The synthesis and use of [18F]-FET and PET imaging was conducted in accordance with current guidelines and as described in our previous studies [23–25]. All patients underwent FET-PET imaging, either by a Gemini GXL® (Philips, Amsterdam, Netherlands) or a Veroes® (Philips, Amsterdam, Netherlands) device. Patients fasted for a minimum of 6 h before intravenous injection of 185 MBq of FET. PET images were acquired 30 min after injection (3-D acquisition). Computed tomography was used for attenuation correction.

Image Analysis

For this study, a single author (JP), blinded to the disease course after imaging, re-analyzed both MRI and [18F]FET-PET data. Decisions were backed by previous assessment of a multidisciplinary tumor board including highly experienced neuroradiologists and neuronuclear medicine physicians. Both structural and perfusion MRI but not FET-PET data were analyzed with Syngo.via® (Siemens, Munich, Germany). Subsequently, structural MRI data were co-registered with [18F]FET-PET data and analyzed via Hermes® workstation (Hermes Medical Solutions, Stockholm, Sweden).

For every patient, the target lesion was defined by delineation of tumor margins based on postcontrast enhancement on T1 MRI or/and hyperintensities on T 2, drawing a 2D region of interest (ROI). Blood vessels, resection cavity and cerebrospinal fluid (CSF) spaces were excluded manually. Perfusion maps (CBV_{mean}, CBF_{mean}, MTT, TTP) were obtained by Syngo MR Neuro Perfusion Engine®. Perfusion maps were normalized ($rCBV_{mean}$, $rCBF_{mean}$, rMTT, rTTP) by drawing a standardized 2 cm circular ROI in the normal-appearing brain tissue of the contralateral hemisphere (relative value = ipsilesional value/contralesional value). While perfusion parameters are related with each other (CBV = CBF * MTT), we analyzed every parameter individually in a later step.

In a second step we fused [18F]FET-PET images with structural MRI data. The previously defined ROIs of the lesion and contralateral normal-appearing brain tissue were copied and used for measurement of standard uptake value (SUV = image activity concentration [Bq/g] · patient weight [g] / injected activity [Bq]). Mean and maximum tumor to brain ratios (TBR_{mean}, TBR_{max}) were calculated by division of target lesions SUV by the SUV of the contralateral normal-appearing brain tissue.

Follow-up and Final Diagnosis

Histopathologic evaluation (resection or biopsy) or radioclinical follow-up confirmed either PD or RN. Regarding WHO grade II gliomas, radiological and clinical assessment had to be stable for at least 12 months to diagnose RN. In case of WHO grades III–IV gliomas, at least 6 months of stable radiologic and clinical follow-up controls were required for confirmation of RN. According to the RANO criteria PD was considered when growth of the target lesions in at least 2 subsequent MRI scans was present, accompanied by clinical deterioration or death of patient (not attributable to other causes than tumor-related ones) [21].

Statistics

For MRI and PET parameters intergroup differences were tested via Mann-Whitney U test. The strength of correlation between individual parameters was assessed by Pearson's correlation coefficient. A coefficient of ≥ 0.7 marked strong, 0.4–0.6 moderate and 0–0.3 weak correlation. Using the final diagnosis as reference, we calculated the area under the curve (AUC) for each single and multiparametric model by receiver operating characteristics (ROC) analysis. Statistical significances of AUC values were tested via Wilcoxon signed-rank test [26]. Optimal cut-offs, sensitivities, specificities, and accuracies for discrimination of PD from RN were obtained by maximization of Youden's index. A likelihood ratio test (= analysis of variance) was performed to evaluate whether a multiparametric model significantly outperforms a single parameter approach for discrimination

between PD and RN. Finally, leave one out cross-validation was performed for all models to account for the small sample size and to assess the classification performance of the models for new unseen data. Fisher's exact test was performed to test the significance of the cross-validated models. R (R Core Team 2022, Version 4.2.2, R Foundation for Statistical Computing, Vienna, Austria) was used for all statistical analyses. A p-value < 0.05 defined statistical significance.

Table 1 Tumor-related characteristics

Tumor-related characteristics, WHO 2016 classification (all patients, $n = 37$)	
Oligodendroglioma, IDH mutant and 1p/19q codeleted	4 (10.8%)
WHO grade II	2
WHO grade III	2
Astrocytoma, IDH mutant	3 (8.1%)
WHO grade II	2
WHO grade III	1
Astrocytoma, IDH wild type	5 (13.5%)
WHO grade II	1
WHO grade III	4
Glioblastoma	24 (64.9%)
Glioblastoma, IDH mutant, WHO grade IV	0
Glioblastoma, IDH wild type, WHO grade IV	24
Other	1 (2.7%)
Diffuse glioma, NOS, WHO grade II	1
Molecular markers	
IDH	
Mutant	4 (10.8%)
Wild type	31 (83.7%)
Not available	2 (5.5%)
MGMT promotor	
Methylated	17 (46%)
Unmethylated	11 (29.7%)
Not available	9 (24.3%)
Therapy	
Radiotherapy	37 (100%)
Re-irradiation	7 (18.9%)
Temozolomide	36 (97%)
Bevacizumab	15 (40.5%)
Re-resection	5 (13.5%)
Histological diagnosis after initial scan	8 (21.6%)
Mean follow-up duration (in months)	14

This table depicts the share of tumor types, molecular markers, and therapy parameters in the study population. In the second column absolute numbers and percentage of total population are given.
WHO world health organization, *IDH* isocitrate dehydrogenase, *NOS* not otherwise specified, *MGMT* O-6-methylguanine-DNA methyltransferase

Table 2 Performance of PWI-MRI/FET-PET parameters for differentiation of progressive disease (PD) from radiation necrosis (RN)

	PD, median (range)	RN, median (range)	p^a	AUC (95% CI)	p^b	Cut-off	Sensitivity (95% CI)	Specificity (95% CI)	Accuracy (95% CI)
rCBV$_{mean}$	1.78 (0.63–3.28)	1.18 (0.24–2.06)	<0.001	0.84 (0.7–0.98)	<0.001	>1.48	0.78 (0.26–0.93)	0.9 (0.3–1)	0.81 (0.68–0.95)
rCBF$_{mean}$	1.48 (0.57–4.39)	0.8 (0.23–3.67)	0.098	0.68 (0.4–0.94)	0.09	–			
rMTT	1.1 (0.28–1.87)	1.04 (0.52–4.31)	0.801	0.47 (0.24–0.7)	0.51				
rTTP	1.01 (0.01–1.07)	1.11 (0.98–2.63)	<0.001	0.87 (0.71–1)	<0.001	<1.06	0.93 (0.3–1)	0.8 (0.5–1)	0.89 (0.84–1)
rTBR$_{mean}$	2.23 (1.27–4.31)	0.97 (0.33–2.35)	<0.001	0.91 (0.78–1)	<0.001	>1.98	0.81 (0.3–1)	0.9 (0.5–1)	0.84 (0.78–0.97)
rTBR$_{max}$	2.28 (1.24–3.49)	1.04 (0.47–2.22)	<0.001	0.89 (0.77–1)	<0.001	>1.65	0.89 (0.44–1)	0.8 (0.4–1)	0.86 (0.65–0.97)
rTBR$_{mean}$ + rCBV$_{mean}$	–			0.96 (0.9–1)	<0.001	–	0.85 (0.7–1)	1 (0.5–1)	0.89 (0.81–1)
rTBR$_{mean}$ + rCBV$_{mean}$ + rTTP				0.98 (0.94–1)	<0.001		1 (0.74–1)	0.91 (0.7–1)	0.97 (0.84–1)
All parameters				0.98 (0.93–1)	<0.001		1 (0.67–1)	0.91 (0.7–1)	0.97 (0.84–1)

PWI-MRI perfusion weighted magnetic resonance imaging, *FET-PET* O-(2-[18F]fluoroethyl-)-l-tyrosine-positron emission tomography, *PD* progressive disease, *RN* radiation necrosis, *CI* confidence interval, *AUC* area under the curve, *rCBV$_{mean}$* mean relative cerebral blood volume, *rCBF$_{mean}$* mean relative cerebral blood flow, *rMTT* relative transit time, *rTTP* relative time to peak, *rTBR$_{mean}$* mean relative tumor to brain ratio, *rTBR$_{max}$* maximum relative tumor to brain ratio, *all* combining all parameters
[a] p values for comparison of median values between PD and RN (Mann–Whitney U test)
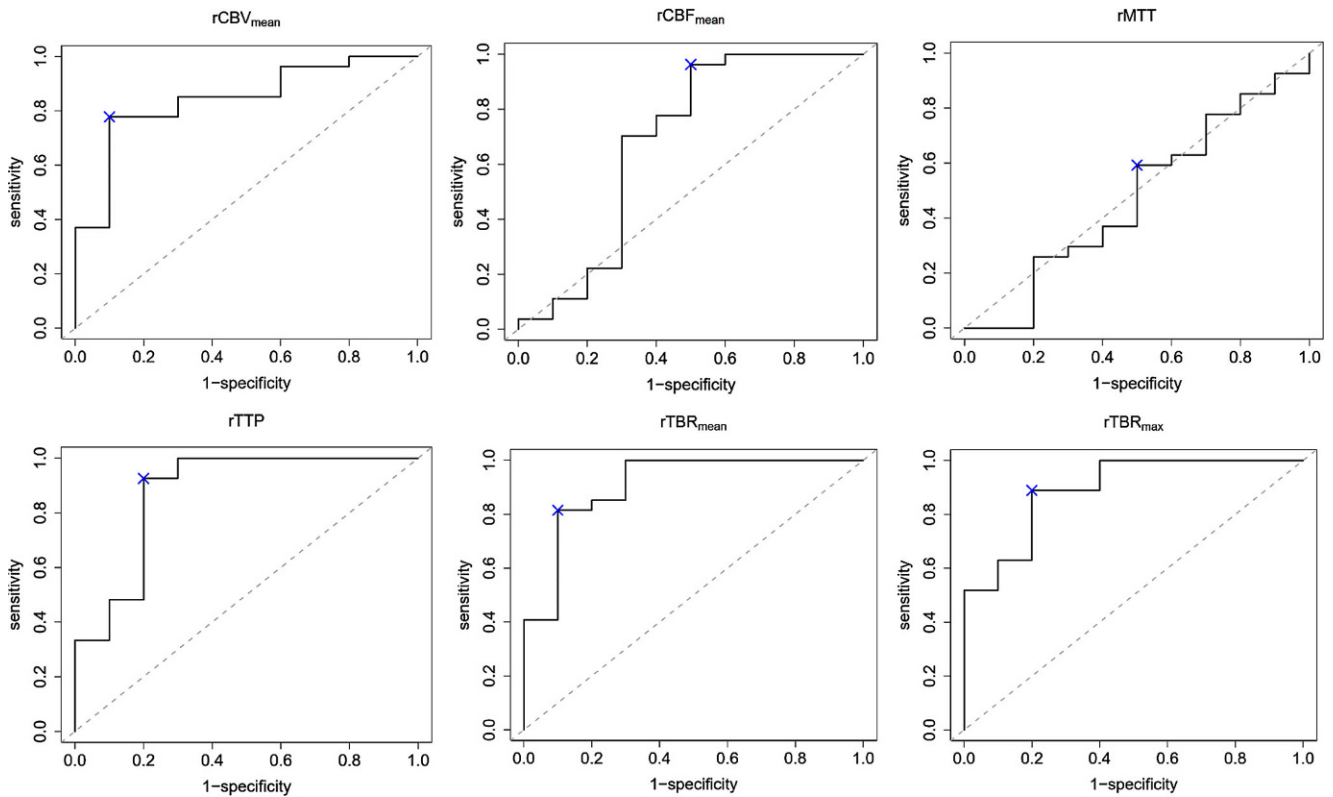[b] p values for the AUC (Wilcoxon signed-rank test)

Fig. 1 ROC curves for PWI-MRI and [18F]FET-PET parameters ROC curves and their respective AUC values for PWI-MRI (rCBV$_{mean}$, rCBV$_{mean}$, rMTT, rTTP) and [18F]FET-PET (TBR$_{mean}$, TBR$_{max}$) parameters for differentiation between progressive disease and radiation necrosis. TBR$_{mean}$ yielded the highest AUC, followed by TBR$_{max}$, rTPP, rCBV$_{mean}$, rCBF$_{mean}$ and rMTT. *ROC* receiver operating characteristic, *PWI-MRI* perfusion weighted magnetic resonance imaging, *[18F]FET-PET* O-(2-[18F]fluoroethyl-)-l-tyrosine-positron emission tomography, *rCBV$_{mean}$* mean relative cerebral blood volume, *rCBF$_{mean}$* mean relative cerebral blood flow, *rMTT* relative mean transit time, *rTTP* relative time to peak, *TBR$_{mean}$* mean tumor to brain ratio, *TBR$_{max}$* maximal tumor to brain ratio, *AUC* area under the curve

Results

Cohort Characteristics

Out of all patients, 37 met the inclusion criteria. We repot a median age of 55 years (range 29–84 years), 51% were female and 49% were male. Of the patients 31 (83.8%) had high grade (WHO grade III or IV) and 6 patients had low-grade (WHO grade II) glioma. Glioblastoma accounted for the highest share of all tumor subtypes (64.9%). In 9 out of 37 patients, MGMT methylation was not identified due to poor quality of the resected tissue. In the remaining 28 patients, the promotor was methylated in 17 (60.7%) and un-methylated in 11 patients (39.3%). RN was found in 6 of 17 patients (35.3%) with a methylated MGMT promotor and in 1 of 10 patients (9.1%) with an unmethylated pro-motor. With respect to the MGMT promotor status, further statistical analysis was not possible due to small subgroups which would have compromised the validity of the results. While all patients received at least one course of radiother-apy prior to initial scanning, 18.9% received at least a sec-ond course. The chemotherapy regimen included temozolo-

mide in 97% and bevacizumab in 40.5% of all patients and 13.5% of all patients received at least a second tumor resec-tion prior to initial scanning. The average interval between initial [18F]FET PET and MRI scan was 5 days. The mean follow-up (based on MRI and clinical assessment) duration was 14 months. Histopathology defined the final diagnosis (PD, $n = 27$; RN, $n = 10$) in 8 cases and radioclinical follow-up in 29. Table 1 summarizes tumor-related characteristics.

Single Parameter Analysis

In PD median values for TBR$_{mean}$ (2.23 vs. 0.97, $p < 0.001$), TBR$_{max}$ (2.28 vs. 1.04, $p < 0.001$) and rCBV$_{mean}$ (1.78 vs. 1.18, $p < 0.001$) were significantly higher and those for rTTP (1.01 vs. 1.11, $p < 0.001$) significantly lower than in RN (Table 2). While median values for rCBF$_{mean}$ (1.48 vs. 0.8, $p = 0.098$) and rMTT (1.1 vs. 1.04, $p = 0.801$) differed between PD and RN, the difference was not statistically significant. In single parameter analysis, rTBR$_{mean}$ (AUC = 0.91, $p < 0.001$), rTBR$_{max}$ (AUC = 0.89, $p < 0.001$), rTTP (AUC = 0.87, $p < 0.001$) and rCBV$_{mean}$ (AUC = 0.84, $p < 0.001$) were efficacious for discrimination of PD from RN
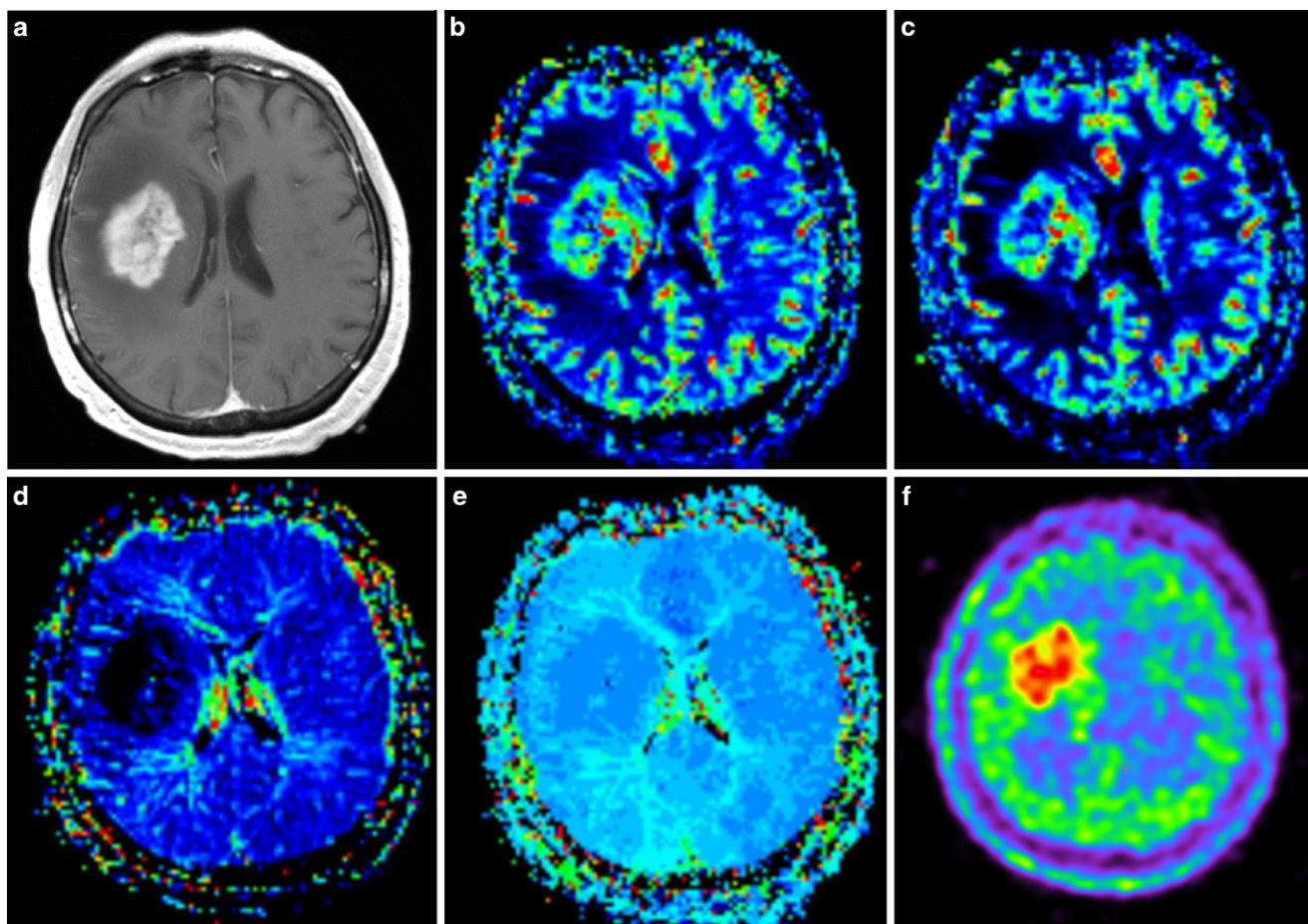
Fig. 2 Progressive disease example of a patient with tumor progression, 7 months after initial diagnosis of anaplastic astrocytoma, resection and chemoradiotherapy the patient clinically deteriorated. Axial T1-weighted contrast-enhanced MRI (**a**) demonstrates right hemispheric progressive tumor tissue, corresponding PWI maps CBV (**b**), CBF (**c**), MTT (**d**), TTP (**e**) and [18F]FET-PET (**f**) imaging are depicted. *MRI* magnetic resonance imaging, *PWI* perfusion weighted imaging, *[18F]FET-PET* O-(2-[18F]fluoroethyl-)-l-tyrosine-positron emission tomography, CBV_{mean} mean cerebral blood volume, CBF_{mean} mean cerebral blood flow, *MTT* mean transit time, *TTP* time to peak, TBR_{mean} mean tumor to brain ratio, TBR_{max} maximal tumor to brain ratio

(Figs. 1, 2 and 3). $rCBF_{mean}$ (AUC = 0.68, $p = 0.09$) and rMTT (AUC = 0.47, $p = 0.51$) did not reach statistical significance. According to Pearson's correlation coefficient, TBR_{mean} and TBR_{max} were highly correlated with each other. Due to the correlation and the higher AUC of the former parameter, TBR_{max} was excluded for further analysis. Optimal cut-offs, sensitivities, specificities, and accuracies for discrimination of PD from RN are given in Table 2.

Multiparametric Analysis

In multiparametric analysis, a classification model consisting of TBR_{mean}, $rCBV_{mean}$ and rTTP achieved an AUC of 0.98 ($p < 0.001$) and significantly outperformed the use of $rTBR_{mean}$ alone ($p = 0.002$), which was the single parametric approach with the highest AUC (Table 2). Exchanging TBR_{mean} for TBR_{max} resulted in the same AUC value, sensitivity, specificity, and accuracy. Adding more parameters did not further increase the AUC. Analysis of variance was performed for the previously mentioned parameters and confirmed that the multiparametric approach was superior to the single parameter one ($p < 0.002$). To assess the considered models in their performances to predict new unseen data, we performed leave one out cross-validation for all models. While cross-validation attributed the highest AUC value to the model consisting of TBR_{mean} and $rCBV_{mean}$, it also suggested that the addition of rTTP resulted in the highest accuracy. Full results of cross-validation were uploaded to the supplement section.

Discussion

Our study evaluated whether a multiparametric classification model combining MRI-PWI and [18F]FET-PET is superior to a single parameter approach to differentiate PD
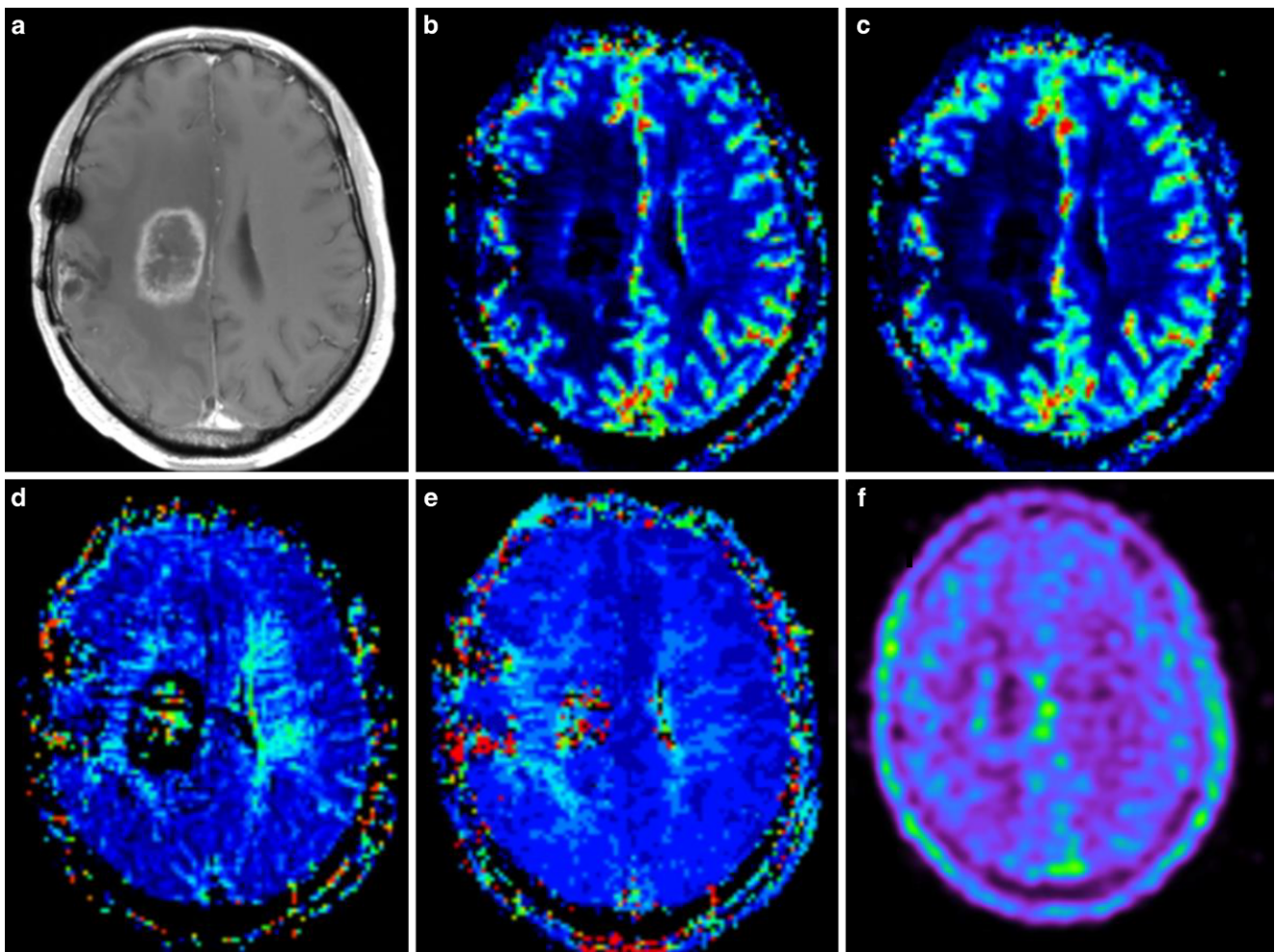
Fig. 3 Radiation necrosis example of a patient with radiation necrosis 20 months after initial diagnosis of glioblastoma, resection and chemoradiotherapy, follow-up imaging showed a new contrast enhancing lesion. Axial T1-weighted contrast-enhanced MRI (**a**) demonstrates right hemispheric necrosis, corresponding PWI maps CBV (**b**), CBF (**c**), MTT (**d**), TTP (**e**) and [18F]FET-PET (**f**) imaging are depicted. *MRI* magnetic resonance imaging, *PWI* perfusion weighted imaging, *[18F]FET-PET* O-(2-[18F]fluoroethyl-)-l-tyrosine-positron emission tomography, *CBV$_{mean}$* mean cerebral blood volume, *CBF$_{mean}$* mean cerebral blood flow, *MTT* mean transit time, *TTP* time to peak, *TBR$_{mean}$* mean tumor to brain ratio, *TBR$_{max}$* maximal tumor to brain ratio

from RN. In single parameter analysis, rTBR$_{mean}$, rTBR$_{max}$, rTTP and rCBV$_{mean}$ were useful for discrimination of PD from RN but rCBF$_{mean}$ and rMTT did not reach statistical significance. In multiparametric analysis, a classification model consisting of rTBR$_{mean}$, rCBV$_{mean}$ and rTTP significantly outperformed the use of rTBR$_{mean}$ alone which was the single parametric approach with the highest AUC. Secondarily, we firstly report the usefulness of rTTP for differentiation of PD from RN.

In single parameter analysis, rTBR$_{mean}$, rTBR$_{max}$, rTTP and rCBV$_{mean}$ were useful for discrimination of PD from RN. The diagnostic performance of TBR (mean and max) and rCBV was similar to previous results [17, 19, 20]. In line with our results, CBF was reported to be not useful for differentiation of PD from RN [27]. As reported previously, in our cohort RN was associated with a higher frequency of

methylated than nonmethylated MGMT status [10]. Kong et al. [10] also showed a difference of rCBV$_{mean}$ between patients with unmethylated MGMT promotor but not in the methylated promotor group. We were not able to verify these findings as small subgroups would have compromised the validity of statistical analysis. We firstly examined the usefulness of PWI rMTT and PWI rTTP for differentiating PD from RN. rMTT was not better than chance in discerning PD from RN. Even though median rTTP was only slightly higher in RN compared to PD, it achieved a moderately high AUC for differentiation PD from RN. As median rCBF$_{mean}$ was lower in RN than in PD, a reduced blood flow and therefore delayed arrival of the contrast agent in necrotic tissue may explain the rTTP increase in RN.

In a second step we assessed the performance of a multiparametric approach. We found maximum AUC for dis-

crimination of PD from RN when combining TBR_{mean}, $rCBV_{mean}$ and rTTP. This model significantly outperformed the use of $rTBR_{mean}$ alone, which was the single parametric approach with the highest AUC. Analysis of variance confirmed the superiority of the multiparametric over the single parameter one. In a final step we performed leave one out cross-validation to assess the robustness of the considered classification models. The approach basically confirmed the results from the multiparametric analysis. The combination of TBR_{mean} and $rCBV_{mean}$ led to the highest AUC value, whereas additionally adding rTTP resulted in the highest accuracy. Overall, multiparametric models showed better discriminating performance than each of the univariate parametric models.

A few studies reported a clear advantage for combined use of MRI-PWI and [18F]FET-PET (TBR), and only under specific circumstances or with at best modest benefit. Pyka et al. (2018) also found increased sensitivity (76%) when combining [18F]FET-PET (TBR) with MRI (ADC+CBV) compared to [18F]FET-PET alone (56%) at a specificity set at 100% [19]. In contrast, we did not focus on maximization of specificity but on AUC, as it encompasses both sensitivity and specificity, making it a more relevant parameter for real-life patient care. Jena et al. (2016) reported increased accuracy (0.91) when combining TBR_{mean} with $rCBV_{mean}$ and maximum accuracy (0.94) when combining TBR_{mean} with $rCBV_{mean}$ and Choline/Creatine ratio [17]; however, this approach was limited by the requirement for magnetic resonance spectroscopy imaging (MRSI). This is an important practical limitation as MRSI is not widely available due to several factors, including increased MRI scanning and post-processing times, low sensitivity and spectral resolution, requirement of expertise for specific voxel techniques, and the danger of metabolite contamination and degradation [28, 29]. Sogani et al. (2017) found increased performance when combining TBR (max and mean) with $rCBV_{mean}$, ADC_{mean} and Choline/Creatine ratio [20]. The practicality of this approach was again limited by the requirement of MRSI for achieving maximum accuracy. The results for a combined use of TBR with PWI without MRSI was not reported. We believe that our classification model is more practical for real-life patient care, as it is not dependent on MRSI. Also, Neuromed Campus, Kepler University Hospital Linz is the sole provider of FET-PET imaging for brain tumors in this federal state (Upper Austria) and bordering areas. Thus, we perform all scans without selection bias in a region encompassing a population of 1.5–2 million people. Thus, we believe to have a more representative patient collective compared to previous studies; however, prospective studies with larger samples are needed to validate our findings.

Limitations

We included both high-grade and low-grade gliomas to increase overall sample size; however, the great majority had high-grade (III–IV) glioma and only a few patients had low-grade (II) glioma, which limited the actual heterogeneity. Due to the rather small sample size, we verified the robustness of our models with leave one out cross-validation. For glioma grading we used the WHO 2016 criteria as the histopathological records date from a timespan when the old classification was in place (2016–2021); however, these grading differences have no actual influence on our results. The use of a hotspot-based method to assess quantitative values limits the reproducibility of our findings. We used this method as our neuroradiologists and neuronuclear medicine physicians have decades of experience with this approach. Instead of creating an artificial study setting we wanted to use the method that is actually used in our routine clinical work. With respect to FET-PET, our study featured only static but not dynamic parameters. As histology was only available in 21.6% of cases, we mainly used radioclinical follow-up for determination of the final diagnosis. While a single author re-analyzed the imaging data, the decisions were backed by a previous assessment of a multidisciplinary tumor board including highly experienced neuroradiologists and neuronuclear medicine physicians.

Conclusion

We report a significant benefit of multiparametric MRI-PWI and [18F]FET-PET over single parameter analysis for discrimination of progressive disease (PD) from radiation necrosis (RN) in patients with glioma. A classification model consisting of TBR_{mean}, $rCBV_{mean}$ and PWI rTTP significantly outperformed the use of $rTBR_{mean}$ alone, which was the best single parametric approach. Secondarily, we firstly report the potential usefulness of PWI rTTP for discrimination of PD from RN in patients with glioma; however, for validation of our findings the conduction of prospective studies with larger patient samples is necessary.

Data availability The datasets are available from the corresponding author on reasonable request.

Declarations

References

1. Tan AC, Ashley DM, López GY, Malinzak M, Friedman HS, Khasraw M. Management of glioblastoma: State of the art and future directions. CA: A Cancer Journal for Clinicians. 2020;70(4):299–312.

2. Siu A, Wind JJ, Iorgulescu JB, Chan TA, Yamada Y, Sherman JH. Radiation necrosis following treatment of high grade glioma—a review of the literature and current understanding. Acta Neurochir. 1. Februar 2012;154(2):191–201.

3. Zikou A, Sioka C, Alexiou GA, Fotopoulos A, Voulgaris S, Argyropoulou MI. Necrosis, Pseudoprogression, Pseudoresponse, and Tumor Recurrence: Imaging Challenges for the Evaluation of Treated Gliomas. Contrast Media Mol Imaging. 2. Dezember. Radiation. 2018;2018:6828396.

4. Ellingson BM, Bendszus M, Boxerman J, Barboriak D, Erickson BJ, Smits M, u. a. Consensus recommendations for a standardized Brain Tumor Imaging Protocol in clinical trials. Neuro-Oncology. 1. September 2015;17(9):1188–98.

5. Shah R, Vattoth S, Jacob R, Manzil FFP, O'Malley JP, Borghei P, et al. Radiation necrosis in the brain: imaging features and differentiation from tumor recurrence. Radiographics. 2012;32(5):1343–59.

6. Nael K, Bauer AH, Hormigo A, Lemole M, Germano IM, Puig J, u. a. Multiparametric MRI for Differentiation of Radiation Necrosis From Recurrent Tumor in Patients With Treated Glioblastoma. American Journal of Roentgenology. 1. Januar 2018;210(1):18–23.

7. Boxerman JL, Ellingson BM, Jeyapalan S, Elinzano H, Harris RJ, Rogg JM, et al. Longitudinal DSC-MRI for Distinguishing Tumor Recurrence From Pseudoprogression in Patients With a High-grade Glioma. Am J Clin Oncol. 2017;40(3):228–34.

8. Young RJ, Gupta A, Shah AD, Graber JJ, Chan TA, Zhang Z, et al. MRI perfusion in determining pseudoprogression in patients with glioblastoma. Clin Imaging. 2013;37(1):41–9.

9. Tsien C, Galbán CJ, Chenevert TL, Johnson TD, Hamstra DA, Sundgren PC, u. a. Parametric response map as an imaging biomarker to distinguish progression from pseudoprogression in high-grade glioma. J Clin Oncol. 1. Mai 2010;28(13):2293–9.

10. Kong DS, Kim ST, Kim EH, Lim DH, Kim WS, Suh YL, et al. Diagnostic Dilemma of Pseudoprogression in the Treatment of Newly Diagnosed Glioblastomas: The Role of Assessing Relative Cerebral Blood Flow Volume and Oxygen-6-Methylguanine-DNA Methyltransferase Promoter Methylation Status. AJNR Am J Neuroradiol. 2011;32(2):382–7.

11. Hu LS, Eschbacher JM, Heiserman JE, Dueck AC, Shapiro WR, Liu S, u. a. Reevaluating the imaging definition of tumor progression: perfusion MRI quantifies recurrent glioblastoma tumor fraction, pseudoprogression, and radiation necrosis to predict survival. Neuro-Oncology. 1. Juli 2012;14(7):919–30.

12. Sugahara T, Korogi Y, Tomiguchi S, Shigematsu Y, Ikushima I, Kira T, et al. Posttherapeutic intraaxial brain tumor: the value of perfusion-sensitive contrast-enhanced MR imaging for differentiating tumor recurrence from nonneoplastic contrast-enhancing tissue. AJNR Am J Neuroradiol. 2000;21(5):901–9.

13. Barajas RF, Chang JS, Segal MR, Parsa AT, McDermott MW, Berger MS, u. a. Differentiation of Recurrent Glioblastoma Multiforme from Radiation Necrosis after External Beam Radiation Therapy with Dynamic Susceptibility-weighted Contrast-enhanced Perfusion MR Imaging1. Radiology. November 2009;253(2):486–96.

14. Henriksen OM, Larsen VA, Muhic A, Hansen AE, Larsson HBW, Poulsen HS, u. a. Simultaneous evaluation of brain tumour metabolism, structure and blood volume using [18F]-fluoroethyltyrosine (FET) PET/MRI: feasibility, agreement and initial experience. Eur J Nucl Med Mol Imaging. 1. Januar 2016;43(1):103–12.

15. Heo YJ, Kim HS, Park JE, Choi CG, Kim SJ. Uninterpretable Dynamic Susceptibility Contrast-Enhanced Perfusion MR Images in Patients with Post-Treatment Glioblastomas: Cross-Validation of Alternative Imaging Options. PLOS ONE. 21. August 2015;10(8):e0136380.

16. Alsop DC, Detre JA. Reduced Transit-Time Sensitivity in Noninvasive Magnetic Resonance Imaging of Human Cerebral Blood Flow. J Cereb Blood Flow Metab. 1. November 1996;16(6):1236–49.

17. Jena A, Taneja S, Gambhir A, Mishra AK, D'souza MM, Verma SM, u. a. Glioma Recurrence Versus Radiation Necrosis: Single-Session Multiparametric Approach Using Simultaneous O-(2-18F-Fluoroethyl)-L-Tyrosine PET/MRI. Clin Nucl Med. Mai 2016;41(5):e228–236.

18. Langen KJ, Galldiks N, Hattingen E, Shah NJ. Advances in neuro-oncology imaging. Nat Rev Neurol. 2017;13(5):279–89.

19. Pyka T, Hiob D, Preibisch C, Gempt J, Wiestler B, Schlegel J, et al. Diagnosis of glioma recurrence using multiparametric dynamic 18F-fluoroethyl-tyrosine PET-MRI. Eur J Radiol. 2018;103:32–7.

20. Sogani SK, Jena A, Taneja S, Gambhir A, Mishra AK, D'Souza MM, et al. Potential for differentiation of glioma recurrence from radionecrosis using integrated 18F-fluoroethyl-L-tyrosine (FET) positron emission tomography/magnetic resonance imaging: A prospective evaluation. Neurol India. 2017;65(2):293–301.

21. Wen PY, Macdonald DR, Reardon DA, Cloughesy TF, Sorensen AG, Galanis E, u. a. Updated response assessment criteria for high-grade gliomas: response assessment in neuro-oncology working group. J Clin Oncol. 10. April 2010;28(11):1963–72.

22. Boxerman JL, Schmainda KM, Weisskoff RM. Relative Cerebral Blood Volume Maps Corrected for Contrast Agent Extravasation Significantly Correlate with Glioma Tumor Grade, Whereas Uncorrected Maps Do Not. AJNR Am J Neuroradiol. 2006;27(4):859–67.

23. Hamacher K, Coenen HH. Efficient routine production of the 18F-labelled amino acid O-2-18F fluoroethyl-L-tyrosine. Appl Radiat Isot. 2002;57(6):853–6.

24. Law I, Albert NL, Arbizu J, Boellaard R, Drzezga A, Galldiks N, et al. Joint EANM/EANO/RANO practice guidelines/SNMMI procedure standards for imaging of gliomas using PET with radiolabelled amino acids and [18F]FDG: version 1.0. Eur J Nucl Med Mol Imaging. 2019;46(3):540–57.

25. Pichler R, Dunzinger A, Wurm G, Pichler J, Weis S, Nußbaumer K, u. a. Is there a place for FET PET in the initial evaluation of brain lesions with unknown significance? Eur J Nucl Med Mol Imaging. 1. August 2010;37(8):1521–8.

26. Hanley JA, McNeil BJ. The meaning and use of the area under a receiver operating characteristic (ROC) curve. Radiology. 1982;143(1):29–36.

27. Larsen VA, Simonsen HJ, Law I, Larsson HBW, Hansen AE. Evaluation of dynamic contrast-enhanced T1-weighted perfusion MRI in the differentiation of tumor recurrence from radiation necrosis. Neuroradiology. 1. März 2013;55(3):361–9.

28. Serkova NJ, Brown MS. Quantitative analysis in magnetic resonance spectroscopy: from metabolic profiling to in vivo biomarkers. Bioanalysis. 2012;4(3):321–41.

29. Chiang GC, Kovanlikaya I, Choi C, Ramakrishna R, Magge R, Shungu DC. Magnetic Resonance Spectroscopy, Positron Emission Tomography and Radiogenomics-Relevance to Glioma. Front Neurol. 2018;9:33.